Calibration of a Quasi-Adiabatic Magneto-Thermal Calorimeter Used to Characterize Magnetic Nanoparticle Heating

Anilchandra Attaluri[1]
Department of Radiation Oncology
and Molecular Radiation Sciences,
Johns Hopkins University School of Medicine,
Baltimore, MD 21287
e-mail: aattalu1@jhmi.edu

Charlie Nusbaum
Department of Applied Physics,
The Richard Stockton College of New Jersey,
Galloway, NJ 08205

Michele Wabler

Robert Ivkov

Department of Radiation Oncology
and Molecular Radiation Sciences,
Johns Hopkins University School of Medicine,
Baltimore, MD 21287

To assess and validate temperature measurement and data analysis techniques for a quasi-adiabatic calorimeter used to measure amplitude-dependent loss power of magnetic nanoparticles exposed to an alternating magnetic field (AMF) at radiofrequencies (160 ± 5 kHz). The data collected and methods developed were used to measure the specific loss power (SLP) for two magnetic iron oxide nanoparticles (IONPs) suspensions, developed for magnetic nanoparticle hyperthermia. Calibration was performed by comparing measured against calculated values of specific absorption rate (SAR) of a copper wire subjected to AMF. Rate of temperature rise from induced eddy currents was measured (n = 4) for a copper wire of radius 0.99 mm and length of 3.38 mm in an AMF at amplitudes (H) of 16, 20, 24, and 28 kA/m. The AMF was generated by applying an alternating current using an 80-kW induction power supply to a capacitance network containing a 13.5-cm vertical solenoid that held the calorimeter. Samples were taped to an optical fiber temperature probe and inserted into a standard (polystyrene, 5 ml) test tube which was suspended in the calorimeter. The sample was subjected to the AMF for 30 s or until the temperature of the sample, increased by 30 °C, recorded at 0.3-s intervals. The SAR of the sample was normalized by $H^2f^{1/2}$, averaged, and compared to theoretical values. Iron (Fe) normalized SLPs of two IONPs (JHU-MION and bionized-nanoferrite (BNF) particles (Micromod Partikeltechnologie, GmbH)) in aqueous suspension were measured in the same setup. We report experimental SAR values for the copper of 2.4 ± 0.1, 4.3 ± 0.2, 6.2 ± 0.1, and 8.5 ± 0.1 W/g compared to theoretical values 3.1 ± 0.1, 4.5 ± 0.2, 6.5 ± 0.1, and 9.2 ± 0.2 W/g at AMF amplitudes of 16 ± 0.1, 20 ± 0.2, 24 ± 0.1, and 28 ± 0.1 kA/m, respectively. Normalized experimental data followed a linear trend approximately parallel to theoretical values with an R^2-value of 0.99. The measured SLPs of the JHU particles are higher than BNF particles within the tested AMF amplitude range of 15 kA/m to 45 kA/m. We demonstrated that copper can be used to calibrate magneto-thermal calorimetric systems used for SLP measurements of magnetic nanoparticles for a field range of 15–28 kA/m at 160 ± 5 kHz. We also note that the electrical conductivity, diameter of copper sample and accuracy, and response time of thermometry constrain calibration to lower amplitudes, highlighting the need for development of standard reference materials for such applications.
[DOI: 10.1115/1.4024273]

Introduction

Magnetic nanoparticle hyperthermia (MNPH) has gained significant interest among researchers and clinicians because it promises a minimally invasive and futuristic option of targeted therapy that may address widely disseminated or metastatic disease [1–3]. A significant amount of research effort is directed to develop nanoparticles for MNPH and to understand its interaction with biological systems [3–8]; however, less attention has been devoted to accurately characterize nanoparticle heating, and to validate methods and equipment for these applications [9–12]. The latter is a prerequisite for reliable quality control and assurance, and for consistent treatment planning; elements that are essential for regulatory approval and clinical translation.

Magnetic nanoparticle hyperthermia relies upon the interaction of nanoparticles and AMFs to generate heat through several potential power loss mechanisms [13–15]. Regardless of mechanism, the amount of heat generated depends upon the concentration and physical properties of the nanoparticles, and on the frequency and amplitude of the magnetic field [9,16]. For clinical translation, reproducible and consistent heating is required for effective therapy and for prescriptive treatment planning [16]. The requirement to create uniform AMF in a large volume of interest (VOI) imposes significant challenges to the engineering design of systems. Currently, the only AMF applicator used in clinical setting is the MFH 300 F® (MagForce, AG, Berlin, Germany) which produces a relatively uniform field in a treatment VOI of 20 cm diameter and aperture height up to 300 mm [17]. Furthermore, achieving uniform particle distributions [16,18–20] within target tissues presents an additional challenge reducing therapeutic effect. If both AMF properties and particle distribution within tissues and organs are spatially heterogeneous the irregular heat output potentially leads to under-treatment of tumors and over-heating normal tissue, degrading therapeutic efficacy, and compromising patient safety. Therefore, accurately characterizing the heat produced, i.e., SLP, over a range of AMF amplitudes provides critical data for biomedical applications.

Heat generated by iron oxide magnetic nanoparticles (IOMNPs) when exposed to an AMF is due to a combination of several potential mechanisms leading to losses during the magnetization reversal process [11–15,21,22]. Hence, the convention of SLP is

[1]Corresponding author.

Manuscript received October 15, 2012; final manuscript received April 11, 2013; published online July 11, 2013. Assoc. Editor: Malisa Sarntinoranont.

considered preferable for magnetic nanoparticles, such as those comprising magnetic iron oxide. Under certain conditions, the power dissipated by a magnetic material subjected to an AMF may be defined as the product of specific losses of the material represented as the area of the hysteresis loop (A_H, related to specific losses of the material) and frequency (f) of the AMF [21,22]. For calorimetric measurements, SLP is defined as the thermal power dissipated by the material per unit mass when it is exposed to AMF having a defined frequency and amplitude. In other words, heat produced by magnetic nanoparticles exposed to AMF is characterized by a normalized loss power that is measured at a given AMF frequency (f) and amplitude (H). Often, this value is reported as a function of either varying AMF frequency (f) or amplitude (H). Typical calorimetric methods used to estimate SLPs of the particles employ an insulated vessel placed within a simple solenoid [15,23]. It is well established, however, that simple solenoids generate inhomogeneous fields; thus, placing severe limitations on both accuracy and precision of such measurements [24,25]. The initial slope of the temperature-versus-time curve is typically used to estimate the SLP generated by a sample using the expression: $\mathrm{SLP} = [C/m_{\mathrm{Fe}}] * [dT/dt],\ as\ t \rightarrow 0$ where m_{Fe} is the mass of iron in the sample for IONPs, C is the heat capacity of the sample, and dT/dt is the measured temperature rate of rise.

Assuming nanoparticle properties are accurately measured (i.e., iron concentration), accuracy and precision of nanoparticle SLP characterization is limited by (1) AMF uniformity in the VOI; (2) uncertainties in measured properties of the calorimeter; and, (3) choice of range of measured data used for analysis. Bordelon et al. [9], describe design and fabrication of a modified solenoid coil for SLP measurements and magnetic nanoparticle hyperthermia in small animals that efficiently generates high amplitude AMF having field uniformity ($\pm 10\%$) within a 125-cm^3 VOI. Bordelon et al. [8], describe a simple but elegant method based on numerical first derivative (slope of T_n–T_{n-1} versus dt) to choose the intervals for fitting to temperature data obtained from a quasi-adiabatic calorimeter to estimate SLP. They associate a positive slope of the T_n–T_{n-1} versus dt curve with thermal mixing within the sample (water absorbing heat, very short duration) whereas, a negative slope occurring later in the heating cycle indicates non-negligible heat losses. Both thermal mixing and non-negligible heat losses negate the thermodynamic assumptions upon which calorimetry are based. Fitting to the data within the interval having slope of the T_n–T_{n-1} versus dt curve approximately zero provides a best estimate of the particle SLP because the zero-slope defines conditions over which thermodynamic assumptions hold true.

Uncertainties in measured properties of the quasi-adiabatic magneto-thermal calorimetric system, described by Bordelon et al. [9], still need to be addressed in order to assess precision of the calorimeter and methods. Also, and perhaps, more important is the requirement that robust and practical methods are yet to be established that enable system calibration to ensure accuracy of data obtained. This can be accomplished by developing methods to calibrate the quasi-adiabatic magneto-thermal calorimetric system over a range of clinically relevant AMF frequency (f) and/or amplitude (H).

Calibrating a magneto-thermal calorimetric system for SLP measurements requires use of a material that generates heat by a known mechanism when exposed to an AMF and for which an analytic expression describing resulting heating exists. Suspensions of magnetic nanoparticles can heat by multiple mechanisms, exhibit concentration dependent heating characteristics due to short- and long-range collective behavior, and possess polydispersity in physical properties [26–28]. These properties, while making the nanoparticles interesting subjects of research, confound development of analytic expressions; thus, precluding their candidacy as standards for calibration.

Conversely, diamagnetic and paramagnetic (nonferromagnetic) materials exhibit negligible (magnetic) hysteresis heating when exposed to AMFs. Nonferromagnetic materials generate Joule heating resulting from finite electrical resistance interacting with eddy or Foucault currents generated within (Faraday's law of induction) the material. This heat generated results from an energy absorption mechanism; hence, the convention of SAR is often adopted. For example, SAR is conventionally applied to tissue heating arising from interactions with electromagnetic fields because tissue temperature rises as power is absorbed via Joule heating from electrical resistance and induced eddy currents. Nonferromagnetic electric conducting bulk materials having precisely measured physical properties make them suitable candidates to calibrate magneto-thermal calorimetric systems. Conversely, complexities of magnetic nanoparticle sample properties that lead to poorly defined heating mechanisms preclude use of nanoparticle suspensions for calibration by SLP measurements. Thompson [29] used aluminum wire to calibrate a setup designed to estimate power deposition in ferrofluid samples over a wide range of AMF frequencies by measuring impedance changes due to the induced power dissipation in the sample. Using copper wire, Natividad et al. [10] performed calibration of an adiabatic magneto-thermal device at a single field amplitude of 1.4 kA/m to measure heat generated by both solid and liquid samples. Further, Natividad et al. [10] used calculated values of field amplitude within a cylindrical volume of 50 cm^3 at the coil center from electromagnetic computer simulations for their measurements. While, both these studies provide guidance, they fail to address the need for calibrating magneto-thermal systems over a range of AMF amplitude at fixed frequency. Further, calculations of AMF amplitude generated by an inductor or solenoid often require assumptions of idealized conditions that may lead to inaccurate estimates of AMF amplitude because AMF system losses (in the resonant circuit, inductor, lead wires, etc.) may not be adequately accounted [8]. Such system losses degrade performance leading to inaccuracies that contribute to inaccurate estimates of SLP, Use of measured current in the inductor, or field amplitude within the VOI is thus required.

Induction heating of a semi-infinite cylindrical nonferromagnetic metal in a uniform AMF is well studied and analytical expressions for calculating total power deposited exist [29,30]. When AMF frequency (f) is less than a certain critical frequency, (f_{crit}), i.e., $f \ll f_{\mathrm{crit}}$, the field inside the nonferromagnetic cylindrical sample is not altered but if AMF frequency is increased such that $f \gg f_{\mathrm{crit}}$, the magnetic field is effectively shielded from the inside of the cylindrical sample due to the induced currents. This phenomenon is also known as skin effect, where the current density is concentrated in a thin layer (penetration or skin depth) on the surface of the cylindrical sample, resulting in higher power dissipation due to the increased resistance to current flow [29,30]. If skin depth (δ) is much less than the radius of the cylindrical sample(r) and $f \gg f_{\mathrm{crit}}$, then the power dissipated P and SAR are given by:

$$P = H^2 \pi r L / \sigma \delta \tag{1}$$

$$\mathrm{SAR} = P/m \tag{2}$$

Here, $\delta = 1/\sqrt{\pi f \mu \sigma}$ is the skin depth of the sample and $f_{\mathrm{crit}} = 1/\pi r^2 \mu \sigma$ is the critical frequency when the radius of the sample is equal to the skin depth. H is the field amplitude of the applied AMF, f is the applied frequency, r is the radius of the sample, m is the mass of the sample, σ is its electrical conductivity, and μ is the magnetic permeability.

Temperature measurements and subsequent analysis of data obtained in quasi-adiabatic RF-calorimeters are commonly used to estimate the amplitude-dependent power loss of magnetic nanoparticles. These data are then reported and used to guide further development of magnetic nanomaterials for biomedical purposes. Often, however, little effort is devoted to accurately characterize and validate the performance of these calorimeters, and few reports provide guidance on choice of methods and materials for

these purposes. Further, no standard reference materials or validated standardized procedures exist.

Here, we describe the use of copper wire and methods to calibrate a previously described quasi-adiabatic magneto-thermal setup capable to generate field amplitude in a range between 2 and 90 kA/m at fixed frequency [8,9]. The field amplitude is explicitly measured using materials and methods already described [8,9]. Performance of the calorimeter is assessed by comparing heating data obtained from copper wire with predicted values calculated using measured AMF properties, copper conductivity, and analytic expressions. We report that while the calorimeter performance is well within predicted values, limitations of precision arise from technologic limitations for measuring temperature and the absence of standard reference materials having wide-ranging electrical conductivity. Following characterization of the calorimeter, we report measurements of the SLP for two representative magnetic IONPs suspensions, developed for magnetic nanoparticle hyperthermia.

Methods and Materials

Copper Sample. Copper wire of diameter about 0.08 in. (hereafter referred to as CU8) were cut from a spool containing 1 m of copper wire and the mass and diameter were subsequently measured using calipers having a precision of ±0.1 mm (Fowler Tools and Instruments, Boston, MA) and an analytical balance having a precision of ±0.1 mg (Mettler Toledo, Columbus, OH). Sample parameters are shown in Table 1. A smaller diameter (0.06 in.) wire was available but was not considered because its radius falls within f/f_{crit} in the range of 1–10 where the corresponding power dissipation is nonlinear (cf. Fig. 2, Ref. [29]).

Iron Oxide Nanoparticles (IONPs). For demonstration, two aqueous IOMNP formulations were used in this study. Suspensions of starch-coated magnetite (Fe_3O_4) core-shell particles (bionized-nanoferrite or BNF-starch, catalog no. 10-00-102) were obtained from micromod Partikeltechnologie, GmbH, Rostock, Germany and used as received. Synthesis procedure and structural and magnetic properties of these particles have been described elsewhere [31–34] and particle size and properties were provided by manufacturer. The iron content, provided by the manufacturer was reported >70% w/w, with a total iron concentration of about 24.3 mg Fe/ml (48 mg particle/ml). Iron concentration of the sample was verified by inductively coupled mass spectrometry (ICP-MS) (data not shown). The particles were suspended in sterile water to provide a stable biocompatible suspension. For SLP measurements, particle suspensions were diluted 1/2 with sterile water SLP.

Suspension of dextran-coated JHU iron oxide core-shell particles were obtained from (Micromod Partikeltechnologie, GmbH, Rostock, Germany). The iron oxide core was prepared separately using a proprietary high-gravity controlled precipitation (HGCP) method (Nanomaterials Technologies, Ltd., Singapore) [35] from aqueous solutions of precursor $FeCl_2$ and NH_4OH. Detailed description of synthesis and particle structure and magnetic characterization are in preparation for publication. The JHU-MION iron oxide cores were dextran coated using methods similar to those described for BNF particles [31] and were used as received. Size and stability of the dextran-JHU-MION particles was provided by manufacturer (cf. Table 1). The particle size distribution based on photon correlation spectroscopy (PCS) is shown in the Fig. 1, and iron concentration of received samples was verified by ICP-MS (data not shown).

Table 1 Available physical parameters for the copper sample and IONPs used in the study

Copper sample properties					
Manufacturer	Stock #/Lot #	Purity	Mass (g)	Diameter (mm)	Length (mm)
ESPI Metals	k1432xy/Q576	3 N	0.0930	1.99	3.379
Magnetic nanoparticle properties					
Name	Manufacturer	Lot #	Iron (mg/ml)	Diameter (nm)	Coating
BNF-starch	Micromod	20711006	24.3	119	Starch
JHU-MIONs	NMT	067114502	13.7	73	Dextran

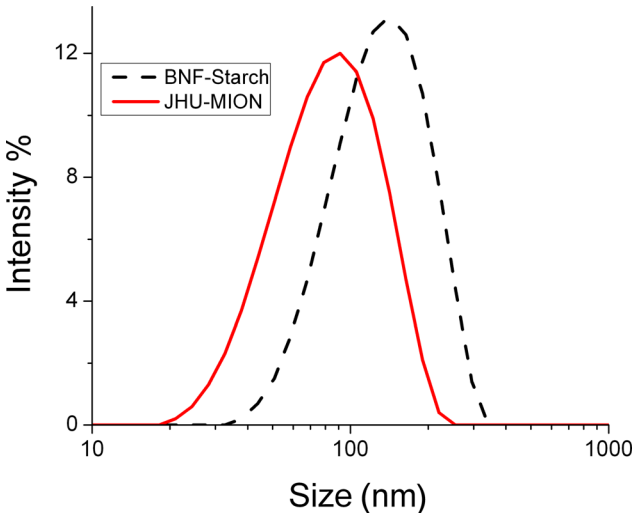

Fig. 1 Magnetic iron oxide particle size distribution based on z-averaged values of intensity obtained from PCS data, as provided by manufacturer.

AMF System. The magneto-thermal setup, described elsewhere [9], produces a uniform AMF (≥90% of peak) over a length of 6.66 cm (125-cm^3 VOI) over AMF amplitude range of 2 kA/m to 90 kA/m and a fixed frequency of 155 ± 10 kHz. A schematic of the magneto-thermal setup is shown in Fig. 2. The insulation chamber, fashioned from Styrofoam, facilitates

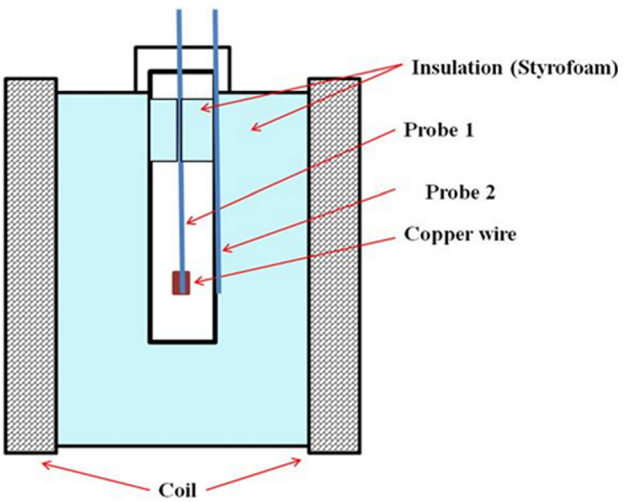

Fig. 2 Schematic of the cross-sectional view of the quasi-adiabatic calorimetric system used for temperature measurements. Two fiber optic temperature probes are shown in the figure. Probe1 is suspended inside the test tube using a Styrofoam (insulation) secured at the top of the tube, while probe 2 is placed at the intersection of surrounding insulation and the 5 ml polystyrene tube.

Table 2 Voltage and frequency information for copper sample experiments and SLP measurements of IONPs

Field (kA/m)	Voltage (V) Probe	Frequency (kHz)	Current (A)
Copper sample experiments			
15.92	2.49	162	292
19.89	3.06	159	306
23.87	3.65	158	322
27.85	4.23	157	339
35.81	5.37	155	370
43.77	6.52	154	395
SLP measurements of IONPs			
15.92	2.53	164	280
19.89	3.08	160	296
23.87	3.65	158	310
27.85	4.20	156	324

positioning of a 5 ml (12 mm diameter) polystyrene test tube such that it is within the uniform AMF. The system is calibrated before each set of experimental runs using a commercial AMF probe (AMF Life Systems, Inc., Auburn Hills, MI), and methods previously described [9]. The calibrated settings are shown in Table 2. Temperatures were measured with fiber optic temperature probes (accuracy: $\pm 0.3\,^{\circ}\mathrm{C}$, resolution: $0.1\,^{\circ}\mathrm{C}$ and response time <750 ms) (FISO Technologies, Ltd., Quebec, Canada), and were recorded at 0.30 s intervals for copper wire and 0.15 s intervals for IONP samples. Samples were subjected to AMF having amplitudes of 16.0 ± 0.1, 20.0 ± 0.2, 24.0 ± 0.1, and 28.0 ± 0.1 kA/m.

Experimental SAR Measurement of CU8. Each copper wire sample was taped to the temperature probe (probe 1) and suspended in an empty 5 ml polystyrene test tube. The observed temperature change when the tape alone was exposed to AMF was within the resolution of the probe. Use of thermal glue/grease was considered in order to decrease contact (thermal) resistance between the probe and CU8 sample. Their use, however, was not pursued to minimize complexity and reduce artifacts. Many thermal grease and glue formulations include silver or graphite to enhance thermal conductivity. As with the copper sample, these materials will interact with the AMFs, generate eddy currents, and deposit heat to the temperature probe complicating data analysis. Further, manufacturers of so-called "off-brand" products rarely provide detailed material composition precluding use. A Styrofoam ring was wrapped around the probe and placed securely within the test tube to suspend the sample and probe and prevent contact with the walls of the test tube. The ring also provides additional thermal insulation. The test tube was then securely placed in the insulating chamber at the center of the vertical coil, creating a quasi-adiabatic system. A second temperature probe (probe 2) was placed at the test tube-styrofoam boundary to record thermal fluctuations arising from heat exchange between the chamber and the water cooled coil. During the short duration (≤ 30 s) of the heating, the observed fluctuations were within the resolution limits of probes. Once secured in the coil, the sample and calorimeter were allowed to thermally equilibrate (defined as temperature variation $\leq \pm 0.2\,^{\circ}\mathrm{C}$ in 30 s) at approximately $21.0 \pm 0.6\,^{\circ}\mathrm{C}$. Thirty seconds after the established criterion for thermal equilibration was achieved, the AMF power was applied and remained on for 30 s or until probe 1 reported a temperature increase of $30\,^{\circ}\mathrm{C}$.

At the conclusion of heating, the power was turned off and the wire was removed from the chamber and cooled by placing the test tube in water maintained at ambient temperature ($\sim 20\,^{\circ}\mathrm{C}$). Sufficient time was given to enable the system to return to thermal equilibrium before each AMF heating cycle. The net temperature change ($dT_{\mathrm{CU}} = T_n - T_o$) and the incremental temperature change (i.e., temperature change between each time step and the immediately preceding time step, $(T_n - T_{n-1})$ were calculated for each Cu8 sample following Bordelon et al. [8]. The appropriate interval for calculating the time-dependent temperature slope for SAR measurement is determined by analysis to define the plateau region of the plot of the incremental temperature change versus dt, which is analogous to the first derivative of the heating rate [8]. The effective net temperature change was calculated by subtracting the net temperature change of the control (probe with tape alone, i.e., no CU8, when exposed to corresponding AMF) from the net temperature change of the CU8 sample ($dT = dT_{\mathrm{CU}} - dT_{\mathrm{control}}$). Once the slope ($dT/dt$) was determined, the experimental SAR of the CU8 sample was calculated using $[C/m_{\mathrm{CU}}] \times [dT/dt]$, where C is the heat capacity of the sample.

Experimental SLP Measurement of IONPs. The 5 ml polystyrene test tube was filled with 1 ml of sample (aqueous suspension) and a fiber optic temperature probe was immersed in the sample to provide optimal thermal contact and minimize systematic error [8,10]. Following Bordelon et al. [8], SLP values were estimated from measured temperature changes. At each power setting, the temperature of a separate 'water blank' containing 1 ml of distilled water was also measured. Water blank temperatures were subtracted from sample temperatures to correct for calorimeter heat capacity. Probe 2 was not used for nanoparticle SLP measurements.

Data Analysis. Weighted least-squares-linear regression was performed (Origin, Northhampton, MA) as described by Bordelon et al. [8] for analysis of both SAR and SLP data. Adjusted R^2 and Pearson's r, values were used to establish acceptance criteria and to evaluate the validity of regression analysis.

Results

Rates of temperature rise (dT/dt) and incremental temperature change ($(T_n - T_{n-1})/dt$) obtained from one trial with the copper sample are shown in Figs. 3(*a*) and 3(*b*), respectively. The plateau region of the rate of incremental temperature change was used to calculate dT/dt as suggested by Bordelon et al. [8] because this is the region for which internal thermal mixing and thermal losses to the environment are negligible. Weighted linear least square regression analysis of the data yielded $R^2 \geq 0.97$.

The SAR values measured for the copper sample at four different AMF amplitude and frequency combinations are shown in Fig. 4. Though the system is considered to be operating at fixed frequency of 160 ± 5 kHz, the frequency varied in a power (voltage) dependent manner (cf. Table 2), as typical for such power supply units. The SAR data are normalized by $H_o^2 f^{1/2}$ to ensure f/f_{crit} assumptions for the analytical expressions are valid. Analytical expressions provided by Zhan [25], and Thompson [24] were used to estimate theoretical values of SAR. The average SAR for each combination of AMF parameters is plotted versus $H^2 f^{1/2}$ (where f is the frequency of the AMF) for comparison with theoretical values.

Slope of the line obtained from regression analysis of the measured amplitude-dependent SAR, i.e., $\mathrm{SAR}(H)_{\mathrm{measured}}$, of the copper sample is similar to the estimated amplitude-dependent SAR, i.e., $\mathrm{SAR}(H)_{\mathrm{estimated}}$, predicted from analytical expression (9.5×10^{-4} versus 9.1×10^{-4}). The ratio of slopes of measured to estimated AMF parameter dependent SAR from Fig. 4 is ~ 1.04, (versus 1 for an ideal case); however, the different y-intercepts (-0.81 versus 0.04) suggests an offset of measured SAR from the estimated values from analytical expressions, indicating a measurement bias or bias error. The difference between measured and estimated values of SAR was $<10\%$, except those measured at amplitude 16.0 kA/m.

Nanoparticle SLP obtained from the two IONPs suspensions are shown in Fig. 5. Regression analysis of ΔT versus Δt produced values of $R^2 \geq 0.99$. A recent study by Kallumadil et al. [23] suggested the use of AMF parameter normalized SLP values known

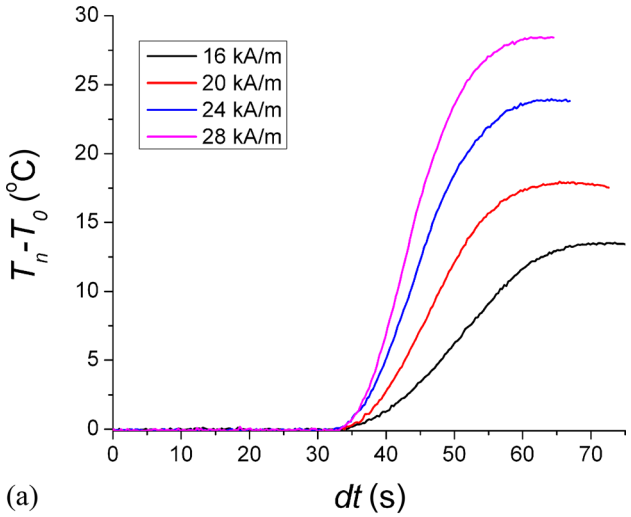

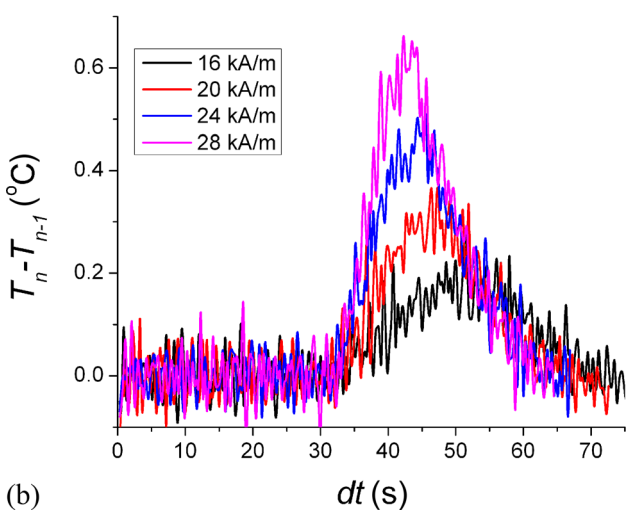

Fig. 3 (*a*) Sample *dT* versus *dt* data of copper sample recorded at four different representative field amplitudes and (*b*) sample incremental temperature change, T_n–T_{n-1}, versus *dt* of copper sample recorded at four different representative field amplitudes.

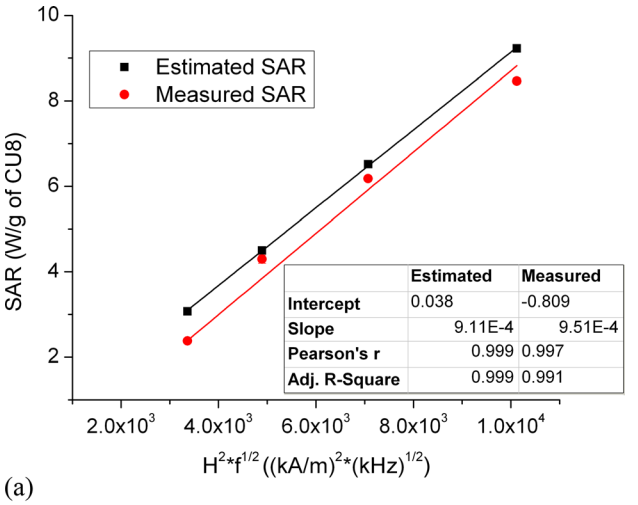

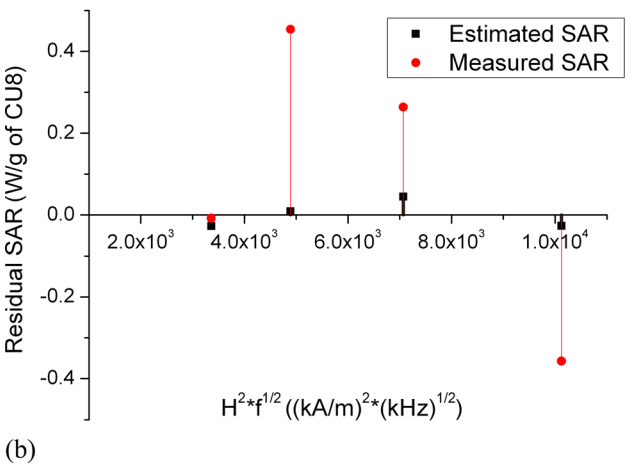

Fig. 4 (*a*) Estimated and measured SAR versus the product of square of field strength and square root of frequency profiles of copper sample. Solid line represents the weighted linear least square regression to the measured SAR data and (*b*) residual of estimated and measured SAR versus the product of square of field strength and square root of frequency profiles of copper sample.

as intrinsic loss of power (ILP) = SLP/H^2f for comparing different nanoparticle formulations. Amplitude-dependent SLPs of BNF-starch and JHU-MIONs are plotted against H^2f (Fig. 5) to represent H^2f normalization of SLP or ILP. The reported SLP values obtained from the JHU particles at the measured amplitude range are higher than those measured for BNFs. Low SLP values from BNF-starch particles determined in this amplitude range are expected because strong inter-particle interactions give rise to high coercivity leading to low SLP at low AMF amplitudes at this frequency, but significant loss power at field amplitudes approaching magnetization saturation [8,28,32–34].

Discussion

Nonferromagnetic materials having well-characterized physical properties are appropriate candidates for calibrating quasi-adiabatic magneto-thermal calorimetric systems. Such materials are ideal because they generate heat by known physical mechanisms when they are exposed to AMFs in the radio-frequency regime. Recent interest in the biomedical applications of magnetic nanoparticle heating with AMFs demands development of reliable methods and standard reference materials to characterize and validate calorimeters and methods used to quantify the heat output of such particles. Magnetic nanoparticles and their suspensions, on the other hand, are unlikely to be suitable for such purposes because of their inherent structural and compositional complexities that inhibit development of accurate analytical expressions. Conversely, nonferromagnetic materials are suitable candidates for characterizing magneto-thermal devices because the physical mechanism (energy absorption) by which they generate heat with exposure to AMF is well-described.

The 80-kW solid-state power supply used in this study is designed to deliver current to a load when resonance criteria are established to maintain a stable frequency between 135 kHz and 440 kHz [9]. As previously described [9], the electromagnetic properties of the resonant circuit and solenoid produced optimal operating frequency of the system at 160 ± 5 kHz. The nature of the calorimeter, sample, and limitations of the temperature recording devices (response time, etc.) limited operation to low power (<5% of maximum power) region of the supply. Stable power delivery was not assured when the system operated at AMF ≤15 kA/m (~1% power). If SAR or SLP measurements require operation at this power range, the instability and attendant variance can propagate as a measurement bias or introduce artifacts.

Operating within the defined limits described above, measured heat output of the copper wire was well within tolerances for SAR estimation (Fig. 4). Measured SAR values are consistently lower

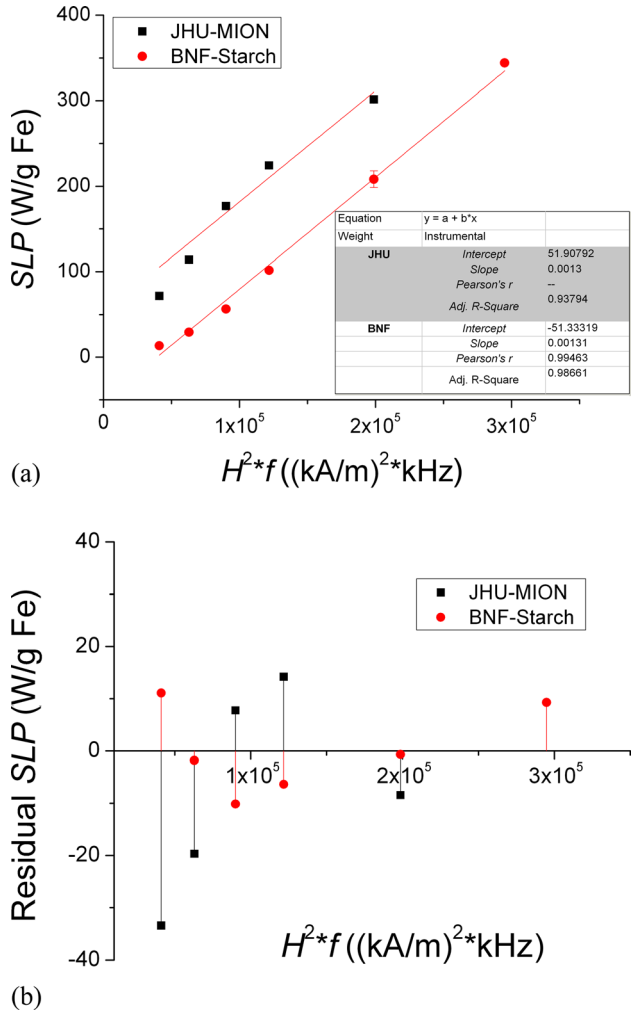

Fig. 5 (*a*) Measured SLPs of BNF-starch and JHU-MIONs over a AMF amplitude range of 15 kA/m to 45 kA/m and (*b*) residual plot of SLPs of BNF-starch and JHU-MIONs

than theoretical SARs, but acceptable because the relative difference or percent difference with respect to estimated SARs is $\leq$10% (Fig. 4). This is true for amplitudes below 16 kA/m, which exceed the above-mentioned lower limit of stable operation of 15 kA/m. At 16 kA/m the measured SAR value was ~22% lower than that of the theoretical SAR. A source for this difference may be the undetectable power fluctuations (instabilities) that occur at low power settings ~15 kA/m. Natividad et al. [10] showed that nonadiabatic determination at amplitude of 1.4 kA/m underestimates the theoretical SAR by 21%. In the present study, the calibration at higher field strengths of 20, 24, and 28 kA/m resulted in reduced difference from the estimated values based on the analytical expressions were 5, 5, and 8%, respectively. The use of measured AMF parameters unlike Natividad et al. [10] could be the reason for reduction in the difference between measured and estimated SARs compared to 21% for nonadiabatic magneto-thermal systems as reported by Natividad et al. [10].

Regression analysis of both measured and estimated amplitude-dependent SARs produces equation(s) of a line having identical slopes (Fig. 4); however, the intercepts differed. This implies a measurement bias or error that does not correlate to precision of measurements. If the estimated amplitude-dependent SARs based on the analytical expression are assumed to provide the true dependence of SAR on AMF parameters, then the regression result of measured amplitude-dependent SARs has a repeatable offset (always lower compared to estimated vales), consistent with a probable systematic error. This measurement bias is unlikely to arise from power supply fluctuations, which are random. Rather, the systematic bias may arise from a discrepancy between the assumed and "true" values for purity and electric conductivity of the copper sample. None of the previous work cited addresses the lack of standard reference material for calibration of magneto-thermal calorimetric systems. Without appropriate characterization of these magneto-thermal calorimetric systems, the quality assurance of the nanoparticle heating/stability is compromised and leads to difficulties in their clinical translation. This underscores the value of appropriate standard reference material development for characterization of magnetic field and calibration of such calorimetric systems.

The methods used in this study to select appropriate data intervals for estimating SLP or SAR are based upon regression analysis of rate of temperature rise or slope of T_n–T_{n-1} versus dt. This analysis, while simple does contain inherent limitations. As with any regression analysis based upon measured values, the result is limited by inherent accuracy and precision of collected data upon which the analysis is based. In the present case, we have identified contributions to these limitations arising from limited response time of temperature probes, power supply instability (at low power), and imprecise knowledge of physical properties of the sample(s). Choice of thermometers is limited by the presence of AMF— only nonconducting materials are appropriate to minimize self-heating of the temperature probe. Fiber optic temperature probes are a technology that has been developed for many applications, including measuring temperatures within oscillating magnetic fields (e.g., magnetic resonance imaging devices). The probes and system chosen for this study are commercially available and facilitate convenient use. By nature, the methods described here also test the validity of the thermometers used, and thus their limitations.

More detailed analysis of the inhomogeneous temperature distribution within the test chamber or nanoparticle samples can be enabled by performing multipoint measurements. Introducing multiple probes with diameter ~1 mm in a small area of ($r \sim 5$ mm) without touching the side walls, however, is technically challenging and would likely introduce thermal variability (artifacts) into the experiment degrading both precision and accuracy. Further, the method used to analyze rate of temperature rise and choose the appropriate region (i.e., zero-slope of derivative of temperature change) makes such multipoint measurements redundant because the zero-slope region defines the region in which there is no thermal mixing in the sample. Thus, the zero-slope region, by nature defines the region at which the sample temperature can be assumed to be uniform (within the response time of the temperature probe) and for which heat losses to the environment are negligible making multipoint measurements unnecessary [8].

The modified solenoid used in the present study generates a uniform field in the VOI, unlike the heterogeneous AMFs generated by simple solenoids. Despite this limitation, simple solenoids are more typically used as research devices for magnetic nanoparticle hyperthermia. It is possible to produce a relatively uniform field within a restricted and defined VOI of a simple solenoid by adjusting the coil length and diameter to be larger than that of the sample. This, however, increases the coil inductance leading to reduced current delivered for a given power input, thereby reducing field amplitude. To restore field amplitude, a larger power supply and larger cooling unit are thus required. These limitations often force a compromise between achievable AMF amplitude with calorimeter design and field homogeneity, leading to compromised precision.

Further complicating matters is the choice to calculate or estimate the field amplitude generated by the inductor which houses the calorimeter. The magnetic field strength is typically calculated using the expression for an idealized infinite solenoid, $H = N*I/L$, where N is the number of turns in the coil, I is the coil current, and L is the coil height. This equation generally overestimates the AMF amplitude and fails to account for field inhomogeneity. It

also fails to account for losses incurred by electrical components in the system, and nonideal inductances in the solenoid itself [9]. These approximations introduce additional and undetermined error into the SLP measurements of the magnetic nanoparticles.

The SLPs reported here were measured for a range of AMF amplitude of 15–45 kA/m. For the BNF-starch sample, regression analysis yielded a value of $R^2 = 0.99$, when represented as ILP. A similar analysis of the JHU-MIONs SLP values yields a R^2 value of 0.94. With further examination, deviation of the data from the weighted linear least square trend line at low amplitude can be observed for JHU-MIONs. This highlights magneto-structural differences between the particles even over small range of 15–36 kA/m AMF amplitudes, emphasizing the necessity of a robust model to predict amplitude-dependent SLPs of IONPs. In future, the SLP measurements should be performed at physiological temperature ranges. The current system baseline temperature is determined by the large cooling system used to compensate for the generated resistive heating produced by the AMF power supply and inductor.

At low heating rates the thermometry is challenged by low signal to noise, thus, challenging the accuracy of the fiber optic probes. This can be overcome by increasing the number of averaging points and/or decreasing the acquisition rate. Specific adjustments require further testing, but with established calibration methods (such as copper wire described in this study) before implementing with nanoparticle samples. At high heating rates, thermometry is limited by the response time of the temperature probes and data recording or processing by electronic components receiving signals from the probe. Limited response time limits the number of data points available for analysis of temperature data.

Further, limiting development of standard methods is the lack of reference materials having defined conductivities and properties amenable to this purpose. Required is a set of standard reference materials having electrical conductivities (10^4–10^8 S/m) to calibrate the magneto-thermal calorimetric systems over a wide range of AMF frequencies and amplitudes. The choice of the diameters of the nonferromagnetic wires should result in $f \ll f_{crit}$ or $\gg f_{crit}$, where the assumptions for the derived analytical expressions are valid [29,30] for clinically applicable frequency values.

Heterogeneous distribution of the nanoparticle in the tissue microenvironment is one of the unavoidable scenarios. Depending on local concentration and particle mobility (internalized or membrane bound) in tissue microenvironment, the SLPs of the particles will vary. Methods required for accurate measurement of SLPs at clinically relevant particle immobilization and concentrations have to be developed.

The present study demonstrates the use of nonferromagnetic materials with appropriate diameter (copper wire) to calibrate a quasi-adiabatic magneto-thermal calorimetric device over a range of AMF parameters. It is critical to have a uniform AMF in a volume where the SAR or SLP measurements are performed. Accurate information on the AMF amplitudes and frequencies in the VOI should be acquired. A careful analysis of acquisition rates and acquisition averaging of the data from the temperature probes is necessary to obtain precise characterization of the heating ability of the samples. Electrical conductivity and diameters of the nonferromagnetic samples should be matched to operate within the limitations of the temperature probes.

Conclusion

Nonferromagnetic materials having precisely characterized thermal and electrical properties can be used to calibrate magneto-thermal calorimetric systems used for SLP measurements of magnetic nanoparticles over a wider AMF frequency and field ranges. A set of standard reference materials with electrical conductivities over a wide range (10^4–10^8 S/m) are needed to calibrate such magneto-thermal calorimetric devices for measuring SLPs of IONPs. The fiber optic technology for temperature measurements in the magneto-thermal setups limits the accurate measurement of SLPs at higher temperature elevation rates. SLPs of the IONPs for magnetic nanoparticle hyperthermia should be measured in more realistic physiological setups (immobilization and concentration).

Acknowledgment

This work was supported by Award No: U54CA143803 from the National Cancer Institute (RI) and from the National Science Foundation (NSF), Award No: 1062975 given to the Institute for NanoBioTechnology at Johns Hopkins University. The content is solely the responsibility of the authors and does not necessarily represent the official views of the National Cancer Institute, the National Institutes of Health, or the National Science Foundation.

References

[1] Johannsen, M., Gneveckow, U., Taymoorian, K., Thiesen, B., Waldöfner, N., Scholz, R., Jung, K., Jordan, A., Wust, P., and Loening, S. A., 2007, "Morbidity and Quality of Life During Thermotherapy Using Magnetic Nanoparticles in Locally Recurrent Prostate Cancer: Results of a Prospective Phase I Trial," Int. J. Hyperthermia, **23**(3), pp. 315–323.

[2] Pankhurst, Q. A., Thanh, N. T. K., Jones, S. K., and Dobson, J., 2009, "Progress in Applications of Magnetic Nanoparticles in Biomedicine," J. Phys. D: Appl. Phys., **42**, p. 224001.

[3] DeNardo, S. J., DeNardo, G. L., Miers, L. A., Natarajan, A., Foreman, A. R., Grüttner, C., Adamson, G. N., and Ivkov, R., 2005, "Development of Tumor Targeting Bioprobes ((^{111})In-Chimeric L6 Monoclonal Antibody Nanoparticles) for Alternating Magnetic Field Cancer Therapy," Clin. Cancer Res., **11**(19 Pt 2), pp. 7087s–7092s.

[4] Khandhar, A. P., Ferguson, R. M., Simon, J. A., and Krishnan, K. M., 2012, "Tailored Magnetic Nanoparticles for Optimizing Magnetic Fluid Hyperthermia," J. Biomed. Mater. Res. Part A, **100**(3), pp. 728–737.

[5] Sonvico, F., Mornet, S., Vasseur, S., Dubernet, C., Jaillard, D., Degrouard, J., Hoebeke, J., Duguet, E., Colombo, P., and Couvreur, P., 2005, "Folate-Conjugated Iron Oxide Nanoparticles for Solid Tumor Targeting as Potential Specific Magnetic Hyperthermia Mediators: Synthesis, Physicochemical Characterization, and *In Vitro* Experiments," Bioconjugate Chem., **16**(5), pp. 1181–1188.

[6] Jordan, A., Wust, P., Scholz, R., Tesche, B., Fahling, H., Mitrovics, T., Vogl, T., Cervós-Navarro, J., and Felix, R., 1996, "Cellular Uptake of Magnetic Fuid Particles and Their Effects on Human Adenocarcinoma Cells Exposed to AC Magnetic Fields *In Vitro*," Int. J. Hyperthermia, **12**(6), pp. 705–722.

[7] Giustini, A. J., Ivkov, R., and Hoopes, P. J., 2011, "Magnetic Nanoparticle Biodistribution Following Intratumoral Administration," Nanotechnology, **22**, p. 345101.

[8] Bordelon, D. E., Cornejo, C., Grüttner, C., Westphal, F., DeWeese, T. L., and Ivkov, R., 2001, "Magnetic Nanoparticle Heating Efficiency Reveals Magneto-Structural Differences When Characterized With Wide Ranging and High Amplitude Alternating Magnetic Fields," J. Appl. Phys., **109**, p. 124904.

[9] Bordelon, D. E., Goldstein, R. C., Nemkov, V. S., Kumar, A., Jackowski, J. K., DeWeese, T. L., and Ivkov, R., 2012, "Modified Solenoid Coil That Efficiently Produces High Amplitude AC Magnetic Fields With Enhanced Uniformity for Biomedical Applications," IEEE Trans. Magn., **48**(1), pp. 47–52.

[10] Natividad, E., Castro, M., and Mediano, A., 2008, "Accurate Measurement of The Specific Absorption Rate Using a Suitable Adiabatic Magnetothemal Setup," Appl. Phys. Lett., **92**, p. 093116.

[11] Natividad, E., Castro, M., and Mediano, A., 2009, "Adiabatic vs. Non-Adiabatic Determination of Specific Absorption Rate of Ferrofluids," J. Magn. Magn. Mater., **321**, pp. 1497–1500.

[12] Bakoglidis, K. D., Simeonidis, K., Sakellari, D., Stefanou, G., and Angelakeris, M., 2012, "Size-Dependent Mechanisms in AC Magnetic Hyperthermia Response of Iron-Oxide Nanoparticles," IEEE Trans. Magn., **48**(4), pp. 1320–1323.

[13] Rosensweig, R. E., 2002, "Heating Magnetic Fluid With Alternating Magnetic field," J. Magn. Magn. Mater., **252**, pp. 370–374.

[14] Lévy, M., Wilhelm, C., Siaugue, J. M., Horner, O., Bacri, J. C., and Gazeau, F., 2008, "Magnetically Induced Hyperthermia: Size-Dependent Heating Power of γ-Fe_2O_3 Nanoparticles," J. Phys. Condens. Matter, **20**, p. 204133.

[15] Li, C. H., Hodgins, P., and Peterson, G. P., 2011, "Experimental Study of Fundamental Mechanisms in Inductive Heating of Ferromagnetic Nanoparticles Suspension (Fe_3O_4 Iron Oxide Ferrofluid)," J. Appl. Phys., **110**, p. 054303.

[16] Wust, P., Gneveckow, U., Johannsen, M., Böhmer, D., Henkel, T., Kahmann, F., Sehouli, J., Felix, R., Ricke, J., and Jordan, A., 2006, "Magnetic Nanoparticles for Interstitial Thermotherapy-Feasibility, Tolerance and Achieved Temperatures," Int. J. Hyperthermia, **22**(8), pp. 673–685.

[17] Gneveckow, U., Jordan, A., Scholz, R., Brüss, V., Waldöfner, N., Ricke, J., Feussner, A., Hildebrandt, B., Rau, B., and Wust, P., 2004, "Description and Characterization of the Novel Hyperthermia and Thermoablation System MFH 300F for Clinical Magnetic Fluid Hyperthermia," Med. Phys., **31**(6), pp. 1444–1451.

[18] Attaluri, A., Ma, R., Qiu, Y., Li, W., and Zhu, L., 2011, "Nanoparticle Distribution and Temperature Elevations in Prostatic Tumours in Mice during Magnetic Nanoparticle Hyperthermia," Int. J. Hyperthermia, **27**(5), pp. 491–502.
[19] Bruners, P., Braunschweig, T., Hodenius, M., Pietsch, H., Penzkofer, T., Baumann, M., Günther, R., Schmitz-Rode, T., and Mahnken, A., 2010, "Thermoablation of Malignant Kidney Tumors Using Magnetic Nanoparticles: An in vivo Feasibility Study in a Rabbit Model," Cardiovasc. Intervent Radiol., **13**(1), pp. 127–134.
[20] Johannsen, M., Thiesen, B., Wust, P., and Jordan, A., 2010, "Magnetic Nanoparticle Hyperthermia for Prostate Cancer," Int. J. Hyperthermia, **26**(8), pp. 790–795.
[21] Mamiya, H., and Jeyadevan, B., 2011, "Hyperthermic Effects of Dissipative Structures of Magnetic Nanoparticles in Large Alternating Magnetic Fields," Scientific Reports, Report No. 1, Article No. 157.
[22] Carrey, J., Mehdaoui, B., and Respaud, M., 2011, "Simple Models for Dynamic Hysteresis Loop Calculations of Magnetic Single-Domain Nanoparticles: Application to Magnetic Hyperthermia Optimization," J. Appl. Phys., **109**, p. 083921.
[23] Kallumadil, M., Tada, M., Nakagawa, T., Abe, M., Southern, P., and Pankhurst, Q. A., 2009, "Suitability of Commercial Colloids for Magnetic Hyperthermia," J. Magn. Magn. Mater., **321**, pp. 1509–1513.
[24] Etheridge, M. L., and Bischof, J. C., 2013, "Optimizing Magnetic Nanoparticle Based Thermal Therapies Within the Physical Limits of Heating," Ann. Biomed. Eng., **41**(1), pp. 78–88.
[25] Huang, S., Wang, S. Y., Gupta, A., Borca-Tasciuc, D. A., and Salon, S. J., 2012, "On the Measurement Technique for Specific Absorption Rate of Nanoparticles in an Alternating Electromagnetic Field," Meas. Sci. Technol., **23**, p. 035701.
[26] Krishnan, K. M., 2010, "Biomedical Nanomagnetics: A Spin Through Possibilities in Imaging, Diagnostics, and Therapy," IEEE Trans. Magn., **46**(7), pp. 2523–2558.
[27] Urtizberea, A., Natividad, E., Arizaga, A., Castro, M., and Mediano, A., 2010, "Specific Absorption Rates and Magnetic Properties of Ferrofluids With Interaction Effects at Low Concentrations," J. Phys. Chem. C, **114**(11), pp. 4916–4922.
[28] Kashevsky, B. E., Kashevsky, S., and Prokhorov, I., 2009, "Magnetodynamics and Self-Organization in Strongly Non-Equilibrium Ferrosuspensions," Solid State Phenom., **152**, pp. 175–181.
[29] Thompson, M. T., 1998, "Simple Models and Measurements of Magnetically Induced Heating Effects in Ferromagnetic Fluids," IEEE Trans. Magn., **34**(5), pp. 3755–3764.
[30] Zahn, M., 1997, "Power Dissipation and MagneticForces on MAGLEV Rebars," IEEE Trans. Magn., **33**(2), pp. 1021–1036.
[31] Grüttner, C., Mueller, K., Teller, J., Westphal, F., Foreman, A., and Ivkov, R., 2007, "Synthesis and Antibody Conjugation of Magnetic Nanoparticles With Improved Specific Power Absorption Rates for Alternating Magnetic Field Cancer Therapy," J. Magn. Magn. Mater., **311**(1), pp. 181–186.
[32] Dennis, C. L., Jackson A. J., Borchers, J. A., Hoopes P. J., Strawbridge. R., Foreman, A. R., van Lierop, J., Grüttner, C., and Ivkov, R., 2009, "Nearly Complete Regression of Tumors Via Collective Behavior of Magnetic Nanoparticles In Hyperthermia," Nanotechnology, **20**(39), p. 395103.
[33] Krycka, K. L., Jackson, A. J., Borchers, J. A., Shih, J., Briber, R., Ivkov, R., Grüttner, C., and Dennis, C. L., 2011, "Internal Magnetic Structure of Dextran Coated Magnetite Nanoparticles in Solution Using Small Angle Neutron Scattering With Polarization Analysis," J. Appl. Phys., **109**(7), 07B513.
[34] Dennis, C. L., Jackson, A. J., Borchers J. A., Ivkov, R., Foreman, A. R., Lau, J. W., Goernitz, E., and Gruettner, C., 2008, "The Influence of Collective Behavior on the Magnetic and Heating Properties of Iron Oxide Nanoparticles," J. Appl. Phys., **103**, 07A319.
[35] Chen, J. F., Wang, Y. H., Guo, F., Wang, X. M., and Zheng, C., 2000, "Synthesis of Nanoparticles With Novel Technology: High-Gravity Reactive Precipitation," Ind. Eng. Chem. Res., **39**(4), pp. 948–954.